Journal of Electroceramics, 9, 37–48, 2002

Control of the Grain Boundary Electrical Features of the Semiconducting $SrTiO_3$ Ceramics Synthesized from Surface-Coated Powders

M.-B. PARK[1], N.-H. CHO[1,*] & C.-D. KIM[2]

[1]*Department of Materials Science and Engineering, Inha University, Inchon 402-751, Korea*
[2]*Division of Ceramics, Korea Institute of Science and Technology, Seoul 136-751, Korea*

Submitted September 27, 2001; Revised August 30, 2002; Accepted August 30, 2002

Abstract. Polycrystalline $SrTi_{0.99}Nb_{0.01}O_3$ (STNO) ceramics were synthesized by hot-press sintering Na-coated semiconducting STNO powders. The chemical and electrical characteristics of the grain boundary of the ceramics were investigated, and their relations were discussed in terms of process parameters. The diffusion coefficients as well as the activation energy of the Na ions near the grain boundary were obtained at particular heat-treatment conditions; it was demonstrated that these values can be used to design specific electrical features of the grain boundary. A systematic variation in the electrical characteristics of the grain boundary with process parameters was observed; it indicates that this synthesis method can be used for fine control over the chemical and electrical properties of the semiconducting ceramics.

Keywords: $SrTiO_3$, semiconducting ceramics, grain boundary, electrical characteristics

1. Introduction

Semiconducting ceramics have been widely used in electronic industries, because of their unique and useful electronic characteristics [1]. The electrical features of polycrystalline semiconducting ceramic devices are in most uses crucially determined by the structural and chemical characteristics of the grain boundary [2]. Many researches have been performed on the relation between the electronic behaviors and the structural and chemical characteristics of the grain boundary to obtain a means of controlling grain boundary features [3–5]. Previous techniques for control of grain boundary features include the segregation of particular additives during sintering (Fig. 1(a)) [6–8] as well as the diffusion of additives along the grain boundary by post-sintering heat-treatment (Fig. 1(b)) [9–11], etc. However, these techniques are in need of tremendous trial and error. In addition, in spite of many previous studies to enhance the understanding of the relation between the grain boundary chemistry and the electrical characteristics, it still remains as an unsolved question. In particular, the effect of process parameters on the chemical and electrical features of the grain boundary has not been fully understood yet. As a result, it's very difficult to obtain fine adjustment of the grain boundary-related properties in polycrystalline semiconducting ceramics.

Recently, there have been a few attempts to control the grain boundary structure and chemistry of the ceramics by sintering surface-coated powders, as shown in Fig. 2 [12–14]. One of the advantages of these techniques is to distribute coating materials along the grain boundary uniformly; in these techniques, the materials coated on the powders are believed to dominantly determine the chemical distribution at the grain boundary of the ceramics. Therefore, the understanding of the defect chemistries of the grain boundary is indispensable for a better design of the grain boundary-dependent electrical characteristics.

In this study, the defect chemistry and electrical characteristics of the grain boundary in semiconducting $SrTi_{0.99}Nb_{0.01}O_3$ (STNO) ceramics, which were

*To whom all correspondence should be addressed.

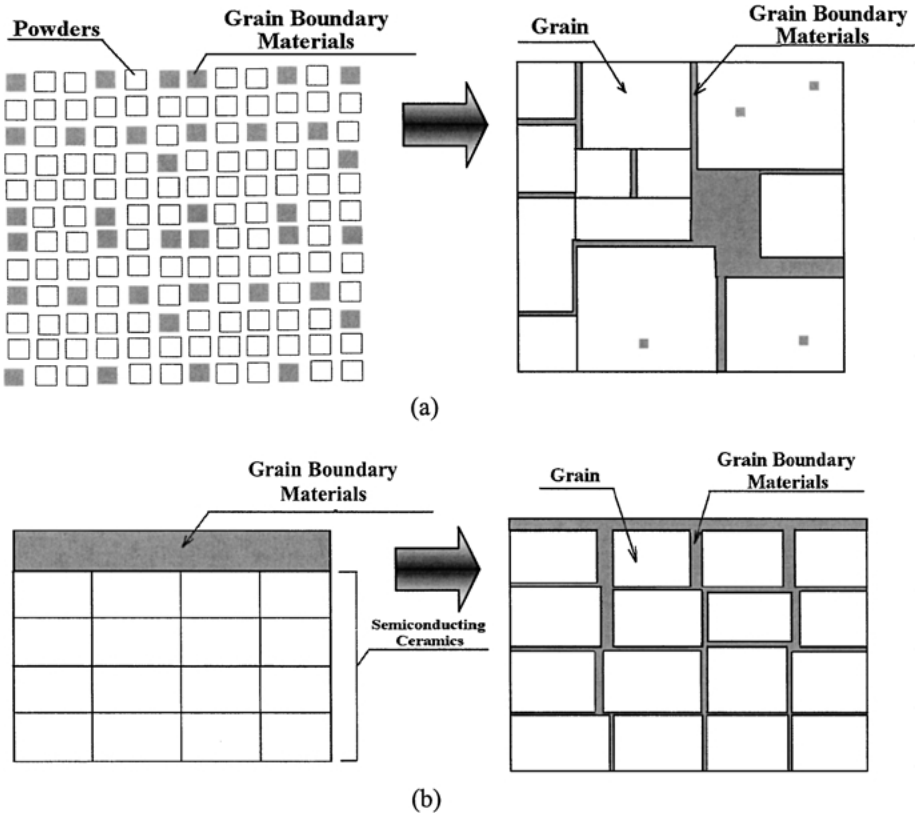

Fig. 1. Schematic diagram of the microstructure and the distribution of grain boundary materials of the ceramics synthesized by traditional techniques. These include the segregation of particular additives (a) and the diffusion of additives along grain boundary by post-sintering heat-treatment (b). (a) The ceramics are synthesized by sintering mixed powders of matrix and grain boundary materials. (b) Grain boundary additives are pasted on the surface of the sintered ceramics, and then a post-sintering heat-treatment is performed.

synthesized from surface-coated powders, were investigated as a function of process parameters such as sintering temperature and time. Kinetic parameters such as diffusion coefficients as well as activation energy of diffusing ions at particular heat-treatment conditions were obtained by fitting experimental data with computer-simulated results, and some work was carried out on the application of these values for the prediction as well as comparison with the experimentally observed grain boundary electrical features of the ceramics.

2. Experimental Procedure

2.1. Preparation of the Semiconducting Oxide Powders

Semiconducting $SrTi_{0.99}Nb_{0.01}O_3$ (STNO) ceramics were prepared with highly pure powders of $SrCO_3$ (99.9%), TiO_2(99.9%) and Nb_2O_5 (99.95%). The constituent powders were mixed according to the stoichiometric ratio for the compound, ball-milled with ethanol media using ZrO_2 balls for 24 hrs, dried at 120°C for 20 hrs, calcined in air at 1100°C for 4 hrs, and ball-milled again. The calcined powders were pressed into disks of 10 mm in diameter under 100 MPa. The green bodies of STNO were sintered at 1550°C, in a reducing atmosphere which was produced by flows of both 10 cm^3/min H_2 and 90 cm^3/min N_2; the reducing atmosphere was applied to produce semiconducting STNO ceramics in this study. The increasing and decreasing rates of furnace temperature were 10°C/min, and the soaking time was 7 hrs. The sintered STNO ceramics consisting of grains with a diameter of approximately 150 μm were crushed, and then semiconducting oxide powders with a diameter range of 1–10 μm were obtained by sedimentation and sieving methods. The size distribution of the semiconducting oxide powders

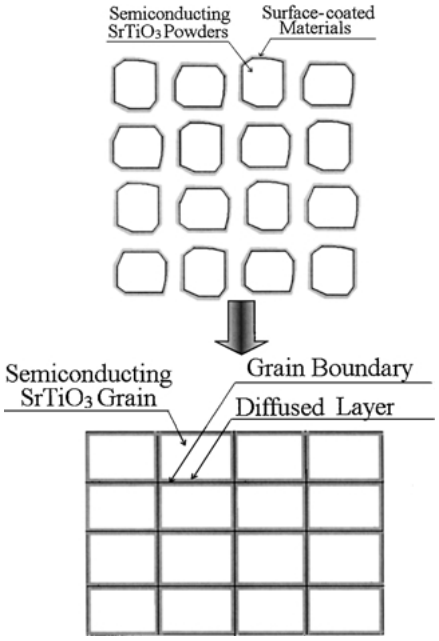

Fig. 2. Schematic diagram of the microstructure and the distribution of grain boundary additives of the ceramics synthesized from surface-coated powders. The ceramics are prepared by hot-press sintering the surface-coated semiconducting powders.

was analyzed using both a photon correlation system (PCS; S4700 Version, Malvern Instrument) and a scanning electron microscope (SEM; X-650, Hitachi); the average size of the powders was 3.1 ± 0.2 μm. Electron diffraction patterns recorded from the powders in this study indicated that the powders are single crystals.

2.2. *Coating and Hot-Press Sintering*

The STNO powders were dispersed in 0.01 M NaOH solutions; the amount of the solutions was chosen so that 5 wt% NaOH can be added to the STNO powders; the wt% of NaOH stands for the weight ratio of NaOH to STNO powders. The solutions were dried in a magnetic hot stirring system at 120°C for 24 hrs; the stirrer was rotated at 200 rpm. After that, they were heat-treated at 300–500°C, so that the absorbed layer became Na_2O [15]. The Na-coated STNO powders were used to produce semiconducting STNO ceramics with chemically-modified grain boundaries. Hot-press sintering of the surface-coated powders was carried out at 1200–1300°C in N_2 atmosphere for 10–60 min under a pressure of 25 MPa; the reducing atmosphere was applied to prevent the semiconducting grains of the ceramics from oxidation.

2.3. *Chemical and Electrical Analysis*

The chemical and structural features of the grain boundary of the STNO ceramics were examined using a transmission electron microscope (TEM; CM200, Philips) with an energy dispersive spectroscopy (EDS; DX4, EDAX) facility; an electron beam probe of 2 nm in diameter was applied for the EDS analysis near the grain boundary. To measure the electrical properties of the ceramics, silver contacts were made on both ends of the disk-shaped sample; the electrode area and the thickness of the sample were 0.16 cm^2 and 0.1 cm, respectively. The complex impedance and the capacitance-voltage (C-V) relations of the ceramics were measured using an impedance analyzer (LF 4194A, Hewlett Packard). Complex impedance analyses were carried out to obtain the resistivity of the grains as well as the grain boundary [16]; ac frequencies ranged from 5 Hz to 13 MHz, and an amplitude of 0.1 V was applied. C-V measurements were performed to acquire the electrostatic potential barrier height of the grain boundary [17]; bias voltage ranged from 0 to 10 V, and a frequency of 1 MHz was applied.

2.4. *Numerical Investigation of Kinetic Parameters*

After hot-press sintering of the green bodies consisting of the powders coated with Na_2O layers with a thickness of b and an initial concentration of C_i^0 is performed for time t, the concentration distribution $C_i(x, t)$ of the coating materials with distance (x) from the grain boundary in the ceramics can be expressed by the following thin film diffusion Eq. (1) [18].

$$C_i(x,t) = \frac{C_i^0}{2}\left[\operatorname{erf}\left(\frac{\frac{b}{2}+x}{2\sqrt{D_i t}}\right) + \operatorname{erf}\left(\frac{\frac{b}{2}-x}{2\sqrt{D_i t}}\right)\right] \quad (1)$$

where $C_i(x, t)$ = concentration of defect i at distance x after annealing for time t; b = thickness of the coating layer; C_i^0 = initial concentration of defect i in the coating layer before annealing; D_i = diffusion coefficient of defect i; t = annealing time; x = distance from the initial coating layer.

The total quantity of the coating materials is fixed throughout the annealing process as shown in the following Eq. (2) [18].

$$\int_{-\infty}^{\infty} C_i(x,t)\,dx = bC_i^0 \tag{2}$$

After annealing for time t, the concentration distribution ($C_i(x,t)$) of the crystal constituents at distance x from the grain boundary can be expressed by the following diffusion Eq. (3) [18].

$$C_i(x,t) = \frac{C_i'}{2}\left[\left\{1+\mathrm{erf}\left(\frac{x-b}{2\sqrt{D_i t}}\right)\right\} + \left\{1+\mathrm{erf}\left(\frac{-x-b}{2\sqrt{D_i t}}\right)\right\}\right] \tag{3}$$

where $C_i(x,t)$ = concentration of defect i at distance x after annealing for time t; b = thickness of the coating layer; C_i' = initial concentration of defect i in the inner region of the grain before annealing; D_i = diffusion coefficient of defect i; t = annealing time; x = distance from the initial coating layer.

Because of the chemical distribution near grain boundary planes, excess effective charges are expected to be distributed in the following way. *pt

$$\rho(x) = \Sigma z_i q C_i(x) \tag{4}$$

where $\rho(x)$ = total charge/unit volume at x; z_i = charge number of defect i; $q = 1.602 \times 10^{-19}$C; $C_i(x)$ = concentration of defect i (e.g. Na'_{Sr}, Na'''_{Ti}, O^{2-}, $V_O^{\cdot\cdot}$, etc.) at x.

Based on the distribution of crystal constituents such as Na, Sr, and Ti as a function of distance from the grain boundary, which were obtained from EDS profiles, diffusion coefficients of the Na, Sr, and Ti were estimated by numerical methods using Eqs. (1)–(3). In this analysis, the lack of constituent elements in the inner region of grains is regarded as being caused by the presence of relevant vacancies and/or substitutional defects; it's assumed that very little interstitial ions exist in the perovskite-structured grains.

3. Results and Discussion

3.1. Chemical Features of the Grain Boundary

Figure 3(a) shows a bright-field image of the hot-press sintered STNO ceramics. The ceramics were prepared from semiconducting STNO powders coated with Na_2O. Figure 3(b) shows the EDS results, which were observed along the line AB in Fig. 3(a). Sr, Ti, O atoms were detected in grains G_1 and G_2, and at the grain boundary. On the contrary, the Na atoms, which were coated on the surface of the powders, were observed at the grain boundary, but not in grains G_1 and G_2. The Na ions coated on the surface of the powders appear to diffuse from the grain boundary to the inner region of the grains, while the other atoms were transported in the reverse direction. With increasing the sintering temperature from 1200 to 1300°C, the amount of diffused atoms near the grain boundary increased, as shown in Fig. 3(c) and (d).

Before hot-press sintering, the coated layer on the surface of the powders is regarded to be composed of Na and O ions; if the molar volume of the coated layer and the powder is assumed to be identical, the composition distribution of the coated layer at the surface of the powders can be illustrated as shown in Fig. 4(a). On the other hand, the hot-press sintering is regarded to cause the coating materials (Na, O) to diffuse into the inner regions of the grains, as shown in Fig. 3(b)–(d). After the hot-press sintering, Sr and Ti deficiency is observed near the grain boundary, while the Na ions are rearranged.

Figure 4(b) shows the fits of the Na ion distribution curves near the grain boundary; these were estimated using Eqs. (1) and (2). The diffusion coefficient of the Na ions, transporting from the coating layer into the inner grain of the STNO ceramics during hot-press sintering at 1250°C, is 4.0×10^{-14} cm^2/sec. Figure 4(c) and (d) shows the fits of the Sr and Ti ion distribution curves near the grain boundary of the STNO ceramics, and these were estimated using Eq. (3). The diffusion coefficients of the Sr and Ti ions, diffusing from the inner region of the STNO grain into the grain boundary during hot-press sintering at 1250°C, are 3.5×10^{-14} cm^2/sec and 2×10^{-14} cm^2/sec, respectively.

Table 1 shows the variation of the diffusion coefficients of the Na, Sr and Ti ions at the grain boundary of the STNO ceramics, which were hot-press sintered at 1200–1300°C. With raising the sintering temperature from 1200 to 1300°C, the diffusion coefficients of the Na, Sr and Ti increased from 1.8, 2.0 and 1.0×10^{-14} cm^2/sec to 7.5, 7.5 and 4.5×10^{-14} cm^2/sec, respectively.

The temperature dependency of the diffusion coefficients of the Na, Sr, and Ti ions near the grain boundary

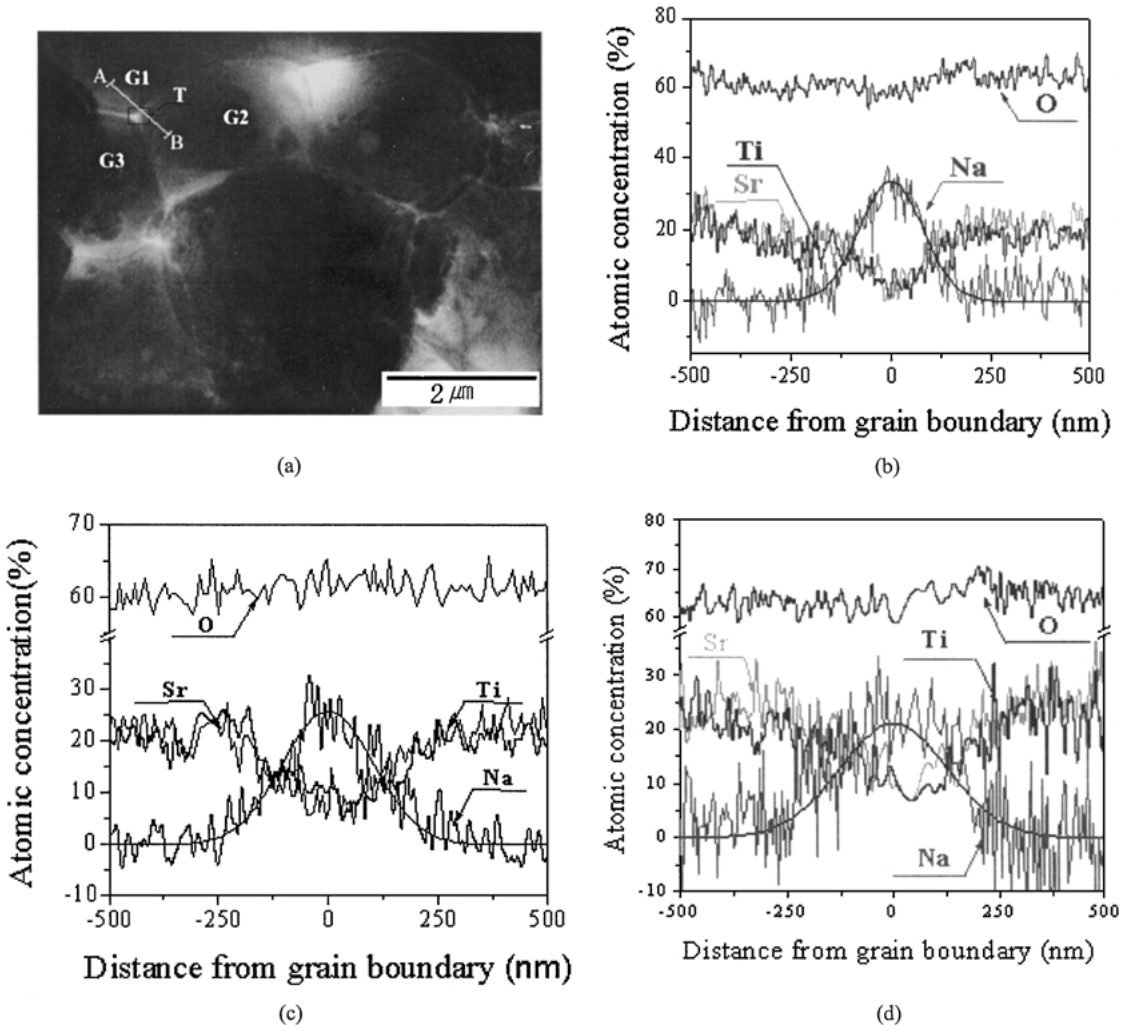

Fig. 3. Microstructure and chemical distribution of the hot-press sintered STNO ceramics. The ceramics were synthesized from 5 wt% NaOH surface-coated powders with a diameter ranging from 1 to 10 μm for 30 min at 1200, 1250, and 1300°C, respectively. (a) Bright-field TEM image of STNO ceramics which were hot-press sintered at 1200°C. (b) Composition profiles along the line AB in (a). (c) and (d) are the composition profiles along a line across the grain boundary of the STNO ceramics, which were hot-press sintered at 1250 and 1300°C, respectively.

can be expressed by the following Eq. (5) [18].

$$D_i = D_i^0 \exp\left(\frac{-Q}{kT}\right) \tag{5}$$

where D_i = diffusion coefficient of defect i; D_i^0 = initial diffusion coefficient; Q = activation energy; k = Boltzmann constant; T = temperature (°K).

Figure 5 shows ln D versus $1/T$ relations for the Na, Sr and Ti ions, where T represents sintering temperature. The diffusion activation energy and initial diffusion coefficients of the Na, Sr and Ti ions can be obtained from the plot in Fig. 5, and the values are listed in Table 1. The activation energy and initial diffusion coefficients of the Na, Sr and Ti ions near the grain boundary, were calculated to be 280, 250 and 290 J/mol and 1.6, 2.0 and 1.8×10^{-4} cm^2/s, respectively. The activation energy of Sr ions is smaller than that of Ti ions, while the initial diffusion coefficient of the former is larger than that of the latter; in general, the diffusion coefficient ($2.0–7.5 \times 10^{-14}$ cm^2/sec) of the former is twice larger than that ($1.0–4.5 \times 10^{-14}$ cm^2/sec) of the latter in the sintering temperature range of 1200–1300°C. It indicates that the amount of Sr ions diffusing

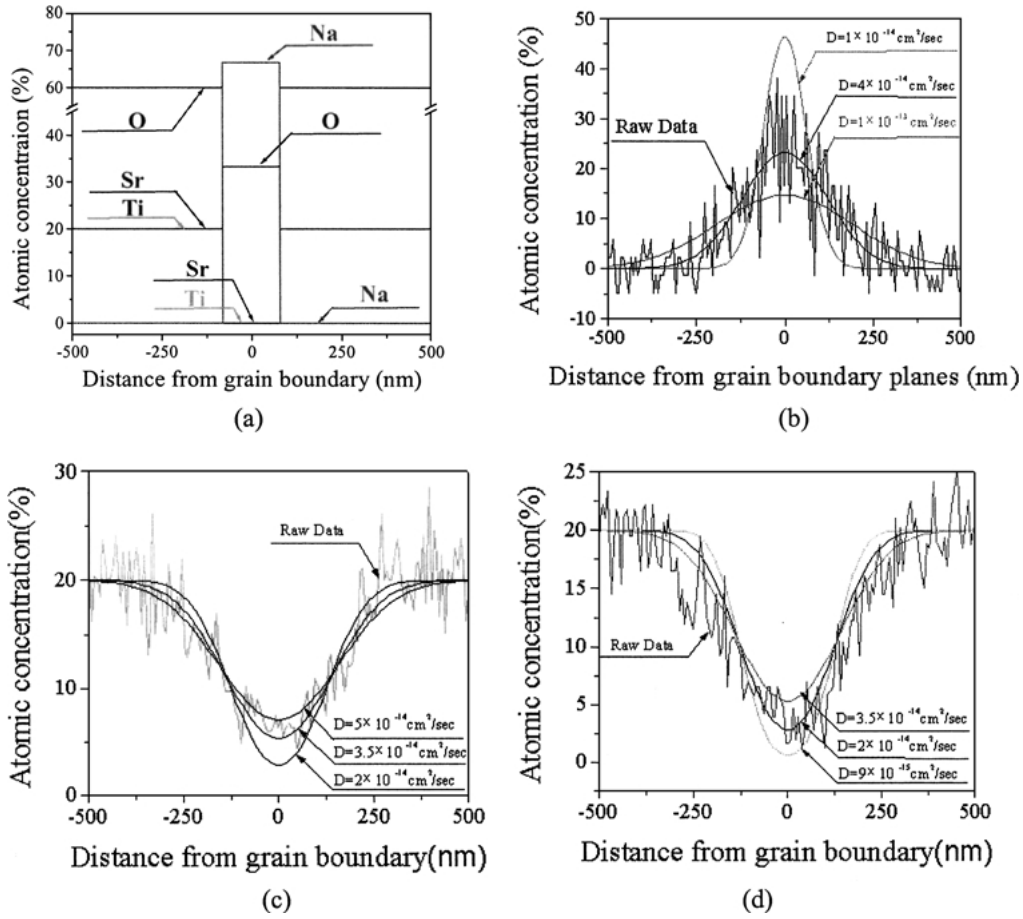

Fig. 4. (a) Schematic illustration of the composition distribution near the grain boundary before hot-press sintering. (b)–(d) EDS composition profiles and corresponding fitting curves near the grain boundary. The composition profiles of the Na, Sr and Ti ions in Fig. 3(c) were fit with the curves simulated at the following conditions; (b) Na ions: $D = 1, 4, 10 \times 10^{-14}$ cm^2/sec, $t = 1800$ sec; (c) Sr ions: $D = 2, 3.5, 5 \times 10^{-14}$ cm^2/sec, $t = 1800$ sec; and (d) Ti ions: $D = 9, 20, 35 \times 10^{-15}$ cm^2/sec, $t = 1800$ sec.

into the grain boundary is larger than that of Ti ions, leaving larger content of Sr vacancies, compared to that of Ti vacancies.

The Na ions were introduced to substitute Sr^{2+} and Ti^{4+} sub-lattices with the aim of modifying the chemical and electrical features of the grain boundary. They formed various defects near the grain boundary; especially, Na'_{Sr} appears to be the main defect near the grain boundary, compared with Na'''_{Ti}, from the fact that the amount of Sr vacancies is larger than that of Ti vacancies. It implies that the former dominantly affect the electrical characteristics of the grain boundary. In addition, the diffusion coefficients of the Na ions are similar to those of the Sr ions; these values are twice larger than that of Ti ions. The difference in ionic radius and electric charge between Na^+(1.02 Å, C.N. = 6) and Ti^{4+}(0.61 Å, C.N. = 6) ions is larger than that between Na^+ and Sr^+(1.26 Å, C.N. = 8) ions [19]. As a result, the formation of Na'''_{Ti} seems to be more difficult than that of Na'_{Sr}.

Figure 6(a) and (b) show the EDS line profiles near the grain boundary of the STNO ceramics, which were hot-press sintered at 1250°C for 10 and 60 min, respectively; these curves were fitted very nicely using Eqs. (1)–(3), with a sintering temperature of $T = 1250$°C (1523 K), sintering time of $t = 600$ and 3600 sec, and diffusion coefficients of $D_{Na} = 4.0 \times 10^{-14}$ cm^2/sec, $D_{Sr} = 3.5 \times 10^{-14}$ cm^2/sec, and $D_{Ti} = 2.0 \times 10^{-14}$ cm^2/sec; these coefficients were obtained for the STNO ceramics which were hot-press sintered at 1250°C for 30 min in this study, as shown in Table 1. The fitting results indicate that the diffusion

Table 1. Variation in the diffusion coefficients, initial diffusion coefficients, and activation energy of the Na, Sr, and Ti ions near the grain boundary of the STNO ceramics with sintering temperature and time.

Ions	Sintering temperature (°C)	Diffusion coefficient, D (10^{-14} cm^2/sec)	Initial diffusion coefficient, D_0 (10^{-4} cm^2/sec)	Activation energy (J/mol)
Na	1200	1.8		
	1250	4.0	1.6	280
	1300	7.5		
Sr	1200	2.0		
	1250	3.5	2.0	250
	1300	7.5		
Ti	1200	1.0		
	1250	2.0	1.8	290
	1300	4.5		

behaviors of the STNO ceramics, synthesized by hot-press sintering Na-coated STNO powders, can be very accurately predicted.

3.2. *Charge Distributions and Electrical Characteristics Near Grain Boundary*

Figure 7 shows the excess negative charge distribution near the grain boundary in the STNO ceramics; these were estimated from Eq. (4) as well as the chemical distribution of Fig. 6. Figure 8(b) shows a schematic diagram of the grain boundary plane indicated with letter m in Fig. 8(a). In region 1, an amorphous phase with a particular width is present, composed of the materials of the coating layers (Na, O). In region 2, various structural defects such as V_{Ti}'''', V_{Sr}'', and $V_O^{\cdot\cdot}$ are located, and in particular the Na^+ ions substitute Sr^{2+} and Ti^{4+} ion sub-lattices, producing defects such as Na_{Sr}' and Na_{Ti}'''. Therefore, excess negative charge layers are regarded to be formed in region 2.

In region 3, the mobile electrons in the conduction band are expected to be depleted, owing to the excess negative charge layers formed in region 2; the total amount of the positive charges in region 3 is equal to that of the excess negative charges in region 2. Region 4 is electrically neutral. As a consequence, the grain boundary electrostatic potential barrier, which is formed due to the net charge density distribution, can be illustrated as shown in Fig. 8(d) [20].

The distribution of the electrostatic potential can be obtained by means of one-dimensional Poission

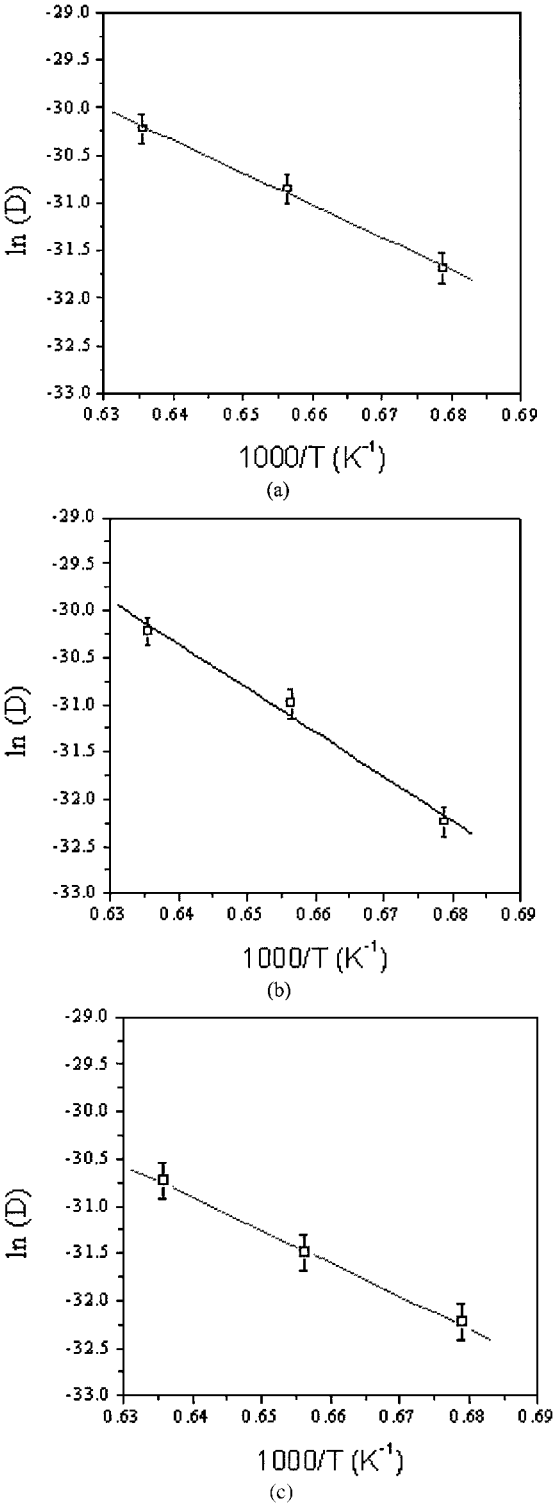

Fig. 5. ln D versus $1/T$ relations of the Na, Sr and Ti ions near the grain boundary; (a) Na ions, (b) Sr ions, and (c) Ti ions.

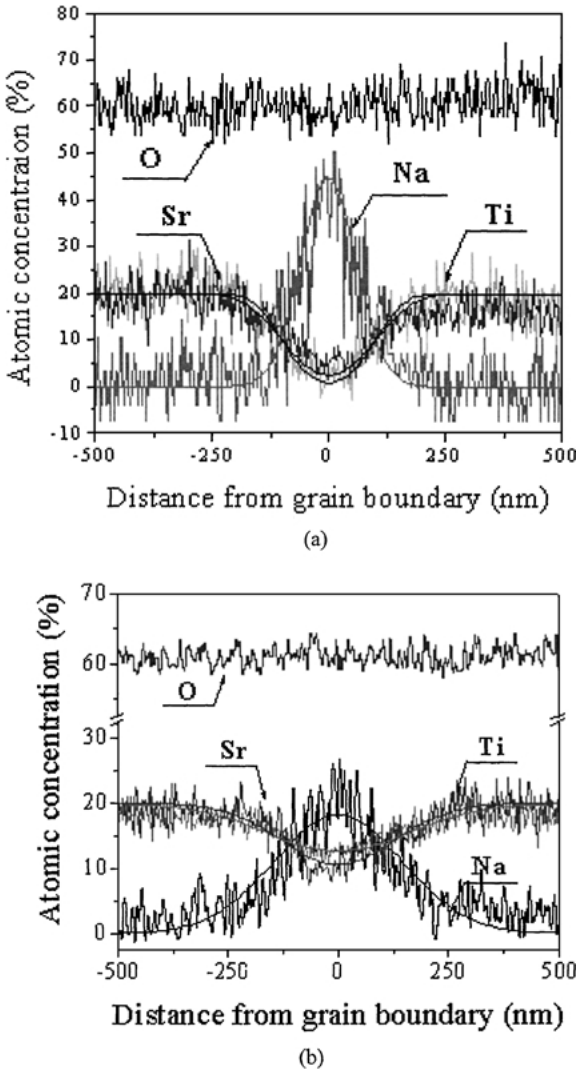

Fig. 6. EDS composition profiles and corresponding fitting curves near the grain boundary, which were hot-press sintered at 1250°C for two different sintering time; (a) 10 min, (b) 60 min. The fitting curves were obtained using Eqs. (1)–(3) at following conditions; Na ions: $D = 4.0 \times 10^{-14}$ cm^2/sec, $t = 600$, 3600 sec; Sr ions: $D = 3.5 \times 10^{-14}$ cm^2/sec, $t = 600$, 3600 sec; Ti ions: $D = 2.0 \times 10^{-14}$ cm^2/sec, $t = 600$, 3600 sec.

Eq. (6) as well as the effective charge density distribution shown in Fig. 7 [21].

$$\frac{\partial^2 \phi(x)}{\partial x^2} = -\frac{\rho(x)}{\varepsilon_s} \tag{6}$$

where $\phi(x) =$ electrostatic potential at x; $\varepsilon_s =$ dielectric constant of $SrTiO_3$ ceramics; $\rho(x) =$ effective charge density.

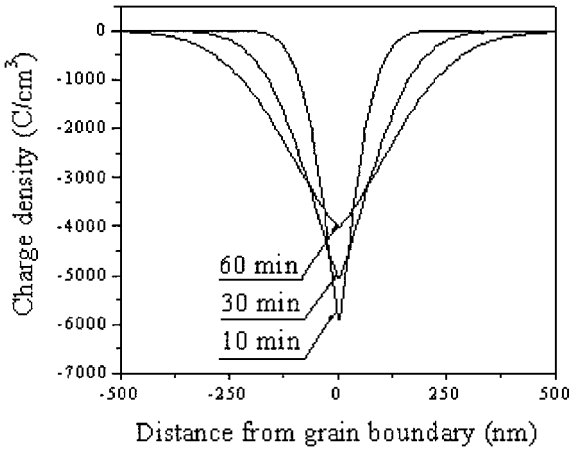

Fig. 7. Distribution of the effective charge density near the grain boundary of the STNO ceramics, which were hot-press sintered at 1250°C for various sintering time; 10, 30, and 60 min, respectively. The curves were estimated from Fig. 3(c) by means of Eq. (4).

Figure 9 shows the variation in the distribution of the electrostatic potential near the grain boundary of the STNO ceramics with sintering time, which were hot-press sintered at 1250°C. In these calculations, region 1 in Fig. 8(b) was considered to be about 150 nm when sintering time was 10 min; this thickness was confirmed in TEM observation. It's very little likely that this region contains effective charges due to the presence of defective chemistry [11, 14]. On the other hand, the boundary region became negligible as sintering time extended up to 30 min. The barrier height increased significantly as the time increased from 10 to 30 min. However, the height changes very little with sintering time larger than 30 min, indicating that the diffusion process reaches its saturation state when $t = 30$ min. Because of the increased diffusion coefficient with raising sintering temperature from 1200 to 1300°C, the width of grain boundary regions (or excess negative charge layers (Table 2), in which 95% of the excess negative charge is present, increased from 240 to 410 nm. The increased diffusion time of Na, Sr and Ti ions near the grain boundary also raised the amount of diffusing materials; with increasing the sintering time from 10 to 60 min, the grain boundary width increased from 210 to 300 nm (Table 2). With varying the sintering temperature and time, the height of grain boundary electrostatic potential barrier changed, and these are listed in Table 2.

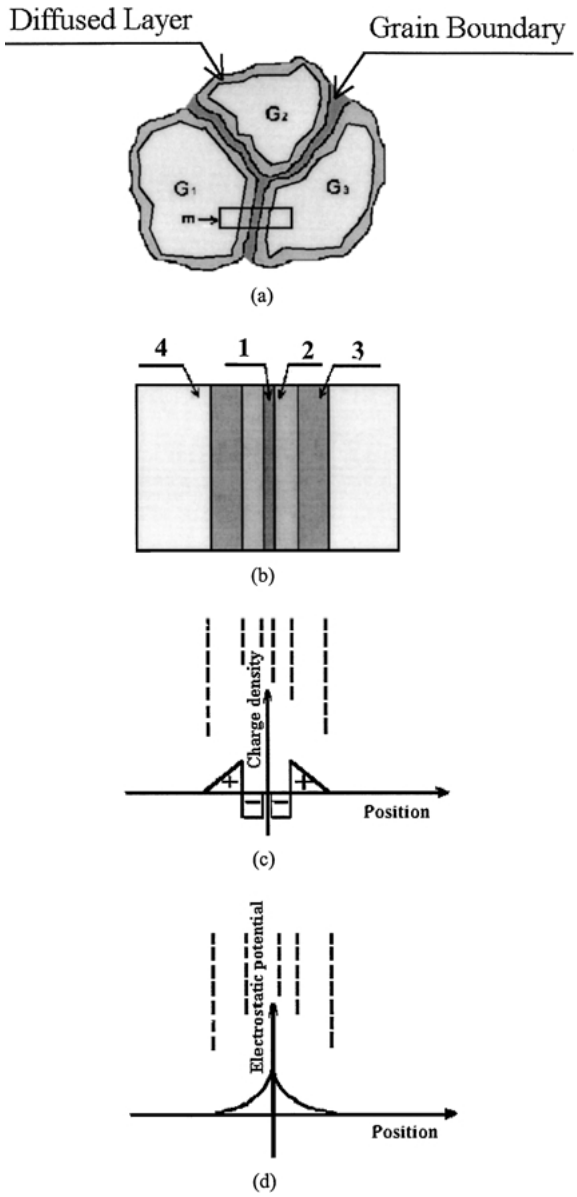

Fig. 8. (a) Schematic illustration of the grain boundary in the STNO ceramics. (b) Enlarged view of the region near the grain boundary plane indicated with letter m in (a), 1: grain boundary plane, 2: excess negative charge layer, 3: depletion layer, 4: bulk region. (c) Charge density distribution. (d) Electrostatic potential distribution.

3.3. *Electrical Characteristics of the STNO Ceramics*

The current versus voltage characteristics of the hot-press sintered STNO ceramics vary with sintering temperature, as shown in Fig. 10(a). Due to the electrostatic potential barrier near the grain boundary, the current versus voltage relation is nonlinear. With increasing the bias voltage, the current increases significantly at a particular voltage. With increasing the sintering temperature from 1200 to 1300°C, the threshold voltage increases from 13 to 19 V/cm; a threshold voltage (Vth) is referred to as an applied voltage at which 1 mA/cm^2 current flows.

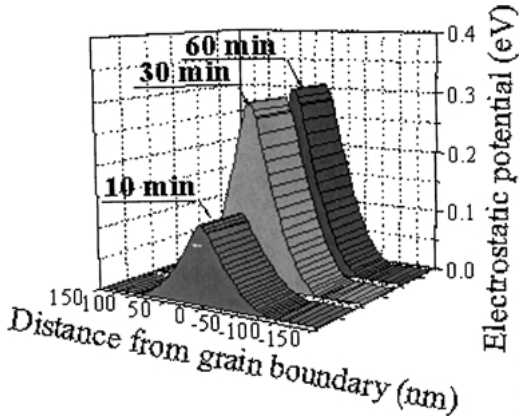

Fig. 9. Distribution of the electrostatic potential of the grain boundary of the STNO ceramics, which were hot-press sintered at 1250°C for various sintering time; 10, 30, and 60 min, respectively.

In the complex-impedance measurement, the resistance values were calculated based on an equivalent circuit consisting of a grain boundary and a grain; a grain boundary is regarded as an electronic device consisting of a resistor and a capacitor being connected in parallel, while a grain is assumed as a resistor; these are connected serially. The grain (R_g) and the grain boundary resistance (R_{gb}) of the sample were obtained from the intercept on the real axis in impedance spectra shown in Fig. 10(b), respectively [16]. The resistance of the grain boundary was converted into a grain boundary resistivity ρ_{gb} using the following relation (7) [16].

$$\rho_{gb} = \frac{LSR_{gb}}{dt} \tag{7}$$

where d = grain boundary layer thickness; L = average grain size; t = sample thickness; S = electrode area; R_{gb} = grain boundary resistance.

The electrode area (S) and thickness (t) of the samples are 0.16 cm^2 and 0.1 cm, respectively. The average grain size (L) is about 3 μm. The thickness (d) of the grain boundary was calculated based on the width of the excess negative charge layer described previously.

Table 2. Numerical work results: Variation in the electrical characteristics of the STNO ceramics with sintering temperature and time.

Sintering temperature (°C)	1200	1250			1300
Sintering time (min)	30	10	30	60	30
Width for 95% negative charge (nm)	240	210	280	300	410
	0.27	0.12	0.29	0.30	0.31
Electrostatic potential barrier height (eV)	$\pm 2 \times 10^{-3}$	$\pm 1 \times 10^{-3}$	$\pm 3 \times 10^{-3}$	$\pm 3 \times 10^{-3}$	$\pm 3 \times 10^{-3}$

With increasing the sintering temperature from 1200 to 1300°C, the grain boundary resistivity increases from 2.2 to 3.0 MΩ·cm, while the grain resistivity remains several Ω·cm; the threshold voltage increases from 13 to 19 V/cm with raising the grain boundary resistivity.

Figure 10(c) shows the capacitance versus voltage relation of the hot-press sintered STNO ceramics. Grain boundary electrostatic potential barrier heights and donor concentrations were obtained from the capacitance versus voltage relation as shown in Eqs. (8) and (9) [17].

$$\left[\frac{1}{C_0} - \frac{1}{2C_0}\right]^2 = \frac{2(\phi + qV)}{(q^2 \varepsilon_s N_D)} \tag{8}$$

$$\frac{1}{C_0} = 2\left[\frac{2\phi}{q^2 \varepsilon_s N_D}\right]^2 \tag{9}$$

where $C =$ capacitance per unit area of grain boundary; $C_0 =$ capacitance at zero applied voltage; $\varepsilon_s =$ dielectric constant of $SrTiO_3$ ceramics; $N_D =$ donor concentration; $\phi =$ grain boundary barrier height; $V =$ applied voltage per grain boundary.

In this measurement, the ceramics were assumed to be composed of uniform cubic grains with an average grain size. Calculation work was conducted using $285 \times \varepsilon_0$ for the dielectric constant (ε) of the $SrTiO_3$ ceramics [22]. With increasing the sintering temperature from 1200 to 1300°C, the electrostatic potential barrier height of the grain boundary increases from 0.28 to 0.31 eV. The variation of the threshold voltage, grain boundary resistivity, and barrier height of the hot-pressed STNO ceramics with sintering temperature is listed in Table 3.

With increasing sintering temperature, the diffusion coefficient of the Na, Sr, and Ti ions near the grain boundary increased, resulting in the increase in the height of electrostatic potential barrier. As a consequence, the threshold voltage, grain boundary resistance, and barrier height of the hot-press sintered STNO ceramics appear to vary with sintering temperature.

Figure 11(a) shows that the current versus voltage characteristics of the STNO ceramics vary with sintering time. With increasing the bias voltage, the current increases significantly at a particular voltage; the current versus voltage relation is nonlinear. The complex impedance spectra and the capacitance versus voltage characteristics of the hot-press sintered STNO ceramics are shown in Fig. 11(b) and (c), respectively. With increasing sintering time from 10 to 60 min, the grain resistivity remains several Ω·cm, while the grain boundary resistivity and the barrier height increase from 2.0 MΩ·cm and 0.12 eV to 3.1 MΩ·cm and 0.30 eV, respectively. With raising the sintering time from 10 to 60 min, the grain boundary resistivity increases from 2.0 to 3.1 MΩ·cm, and as a result, the threshold voltage significantly increases

Table 3. Experimental work results: Variation in the electrical characteristics of the STNO ceramics with sintering temperature and time.

Sintering temperature (°C)	1200	1250			1300
Sintering time (min)	30	10	30	60	30
Grain boundary resistance (kΩ)	12.0	11.2	13.0	17.3	16.5
Grain boundary resistivity (MΩ·cm)	2.2	2.0	2.3	3.1	3.0
	0.28	0.12	0.29	0.30	0.31
Barrier height (eV)	$\pm 3 \times 10^{-3}$	$\pm 1 \times 10^{-3}$	$\pm 3 \times 10^{-3}$	$\pm 3 \times 10^{-3}$	$\pm 3 \times 10^{-3}$
	1.2	1.2	1.2	1.2	1.2
Donor concentration (10^{19}/cm^3)	$\pm 1 \times 10^{-2}$	$\pm 2 \times 10^{-2}$	$\pm 1 \times 10^{-2}$	$\pm 1 \times 10^{-2}$	$\pm 1 \times 10^{-2}$

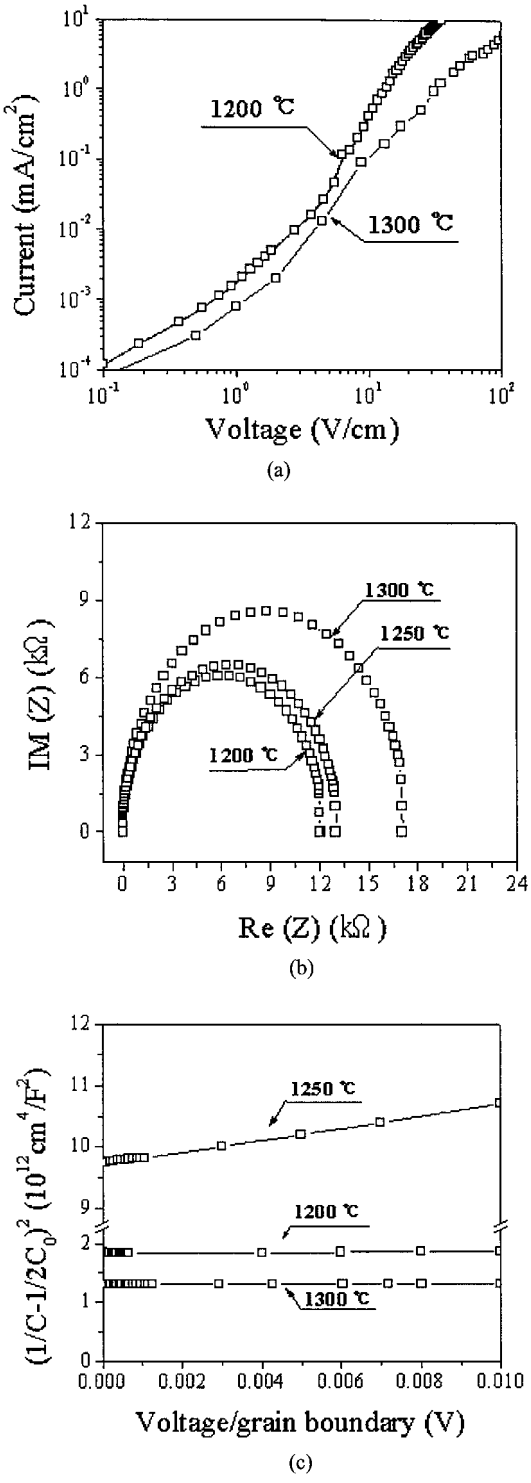

Fig. 10. Variation in the electrical characteristics of the hot-press sintered STNO ceramics for 30 min with sintering temperature; (a) *I-V* relation, (b) complex impedance spectra, and (c) *C-V* relation.

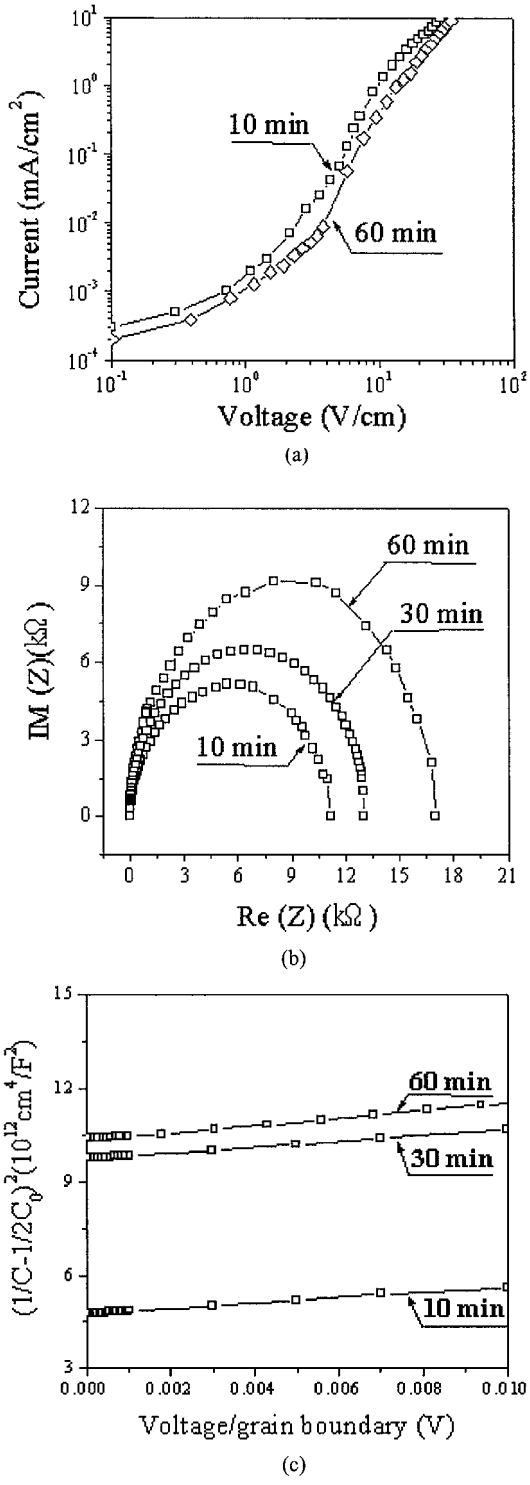

Fig. 11. Variation in the electrical characteristics of the hot-press sintered STNO ceramics at 1250°C with sintering time; (a) *I-V* relation, (b) complex impedance spectra, and (c) *C-V* relation.

from 9.6 to 14 V/cm with raising the grain boundary resistivity.

With increasing sintering time from 10 to 30 min, the amount of diffusion of Na, Sr, and Ti ions near the grain boundary is considered to rise remarkably, resulting in the increase in the electrostatic potential barrier height from 0.12 to 0.29 eV. On the other hand, with raising the sintering time from 30 to 60 min, the electrostatic potential barrier height increased a little, from 0.29 to 0.30 eV, indicating that it takes about 30 min for the system to achieve its nearly final state at a sintering temperature of 1250°C.

The electrostatic potential barrier (Table 2), calculated from the chemical composition obtained at the grain boundary, was similar to that (Table 3) obtained by impedance analysis. The electrical characteristics of the STNO ceramics can be designed and controlled by adjusting the chemical and electrical features of the grain boundary with process parameters.

4. Conclusions

Polycrystalline $SrTi_{0.99}Nb_{0.01}O_3$ (STNO) ceramics were synthesized by hot-press sintering surface-coated semiconducting STNO powders. The materials coated on the powder surface were present near the grain boundary of the ceramics. Because of the excess negative electrical charges formed by the distribution of the structural defects near the grain boundary, electrostatic potential barriers were formed; the electrostatic potential barrier heights were measured in terms of the process parameters, such as sintering temperature and time.

The electrical characteristics of the STNO ceramics can be controlled by adjusting the chemical and electrical features of the grain boundary with process parameters. In particular, the diffusion coefficients and activation energy were obtained from a fitting process for particular heat-treatment conditions. The details of the distribution of diffusing materials as well as structural defects were anticipated, based on the thermodynamic values; these were well-agreed with experimental results, indicating that electrical features of the ceramics consisting of the grain boundary can be designed.

References

1. B.M. Kulwicki, *J. Phys. Chem. Solids*, **45**, 1015 (1984).
2. L. Hozer, *Semiconductor Ceramics: Grain Boundary Effects* (Ellis Horwood, New York, London, Toronto, Sydney, Tokyo, and Singapore, 1994).
3. K. Prume, R. Waser, K. Franken, and H.R. Maier, *J. Am. Ceram. Soc.*, **83**, 1153 (2000).
4. R. Hagenbeck and R. Waser, *J. Appl. Phys.*, **83**, 2083 (1998).
5. A.C. Caballero, J.F. Fernandez, C. Moure, P. Duran, and Y.-M. Chiang, *J. Am. Ceram. Soc.*, **81**, 939 (1998).
6. P.E.C. Franken, M.P.A. Viegers, and A.P. Gehring, *J. Am. Ceram. Soc.*, **64**, 687 (1981).
7. S.B. Desu and D.A. Payne, *J. Am. Ceram. Soc.*, **73**, 3407 (1990).
8. J. Daniel and K.H. Härdtl, *Philips Res. Repts.*, **31**, 487 (1976).
9. M. Fujimoto, Y.-M. Chiang, A. Roshko, and W.D. Kingery, *J. Am. Ceram. Soc.*, **68**, C300 (1985).
10. P.E.C. Franken, M.P.A. Viegers, and A.P. Gehring, *J. Am. Ceram. Soc.*, **68**, 169–173 (1981).
11. M. Fujimoto, Y.-M. Chiang, A. Roshko, and W.D. Kingery, *J. Am. Ceram. Soc.*, **68**, 169 (1985).
12. F.A. Selmi and V.R.W. Amarakoon, *J. Am. Ceram. Soc.*, **71**, 934 (1988).
13. L. Schneider-Stormann, M. Vollmannm, and R. Waser, *Solid State Ionics*, **75**, 123 (1995).
14. M.-B. Park and N.-H. Cho, *J. Am. Ceram. Soc.*, **84**, 1937 (2001).
15. G.C. Matti and M. Baerns, *Appl. Catal. A*, **127**, 219 (1995).
16. K.R. Gerhardt and A.S. Nowick, *J. Am. Ceram. Soc.*, **69**, 641 (1986).
17. K. Maker, K. Tsuda, and I. Nagaswa, *J. Am. Ceram. Soc.*, **50**, 4475 (1979).
18. H. Schmalzried, *Solid State Reactions* (Academic Press, New York and Verlag Chemie, 1974).
19. D.R. Lide, *CRC Handbook of Chemistry and Physics*, 74th Edition (CRC Press, Boca Raton, Ann Arbor, London, and Tokyo, 1993).
20. L. Tian and R. Dieckmann, *J. Non-Crystal. Solids*, **265**, 36 (2000).
21. B.G. Streetman and S. Banerjee, *Solid State Electronic Devices*, 5th Edition (Prentice-Hall, 2000).
22. A.J. Moulson and J.M. Hebert, *Electoceramics: Materials, Properties, Application* (Chapman and Hall, 1992).